Vibration Compensating Beam Scanning Interferometer for Surface Measurement

Haydn Martin, Kaiwei Wang, and Xiangqian Jiang,*

University of Huddersfield, Queensgate, Huddersfield, West Yorkshire, HD1 3DH, England

**Corresponding author: x.jiang@hud.ac.uk*

Light beam scanning using a dispersive element and wavelength tuning is coupled with fiber-optic interferometry to realize a new surface measurement instrument. The instrument is capable of measuring nano-scale surface structures and form deviation. It features active vibration compensation and a small optical probe size that may be placed remotely from the main apparatus. Active vibration compensation is provided by the multiplexing of two interferometers with near common paths. Closed loop control of a mirror mounted on a piezoelectric transducer is used to keep the path length stable. Experiments were carried out due deduce the effectiveness of the vibration compensation and the ability to carry out a real measurement in the face of large environmental disturbance.

OCIS codes: 120.0120, 060.2370, 250.0250, 120.3180.

1. Introduction

Technological advances in several fields have resulted in the increased use of nano-scale and ultra-precision surfaces. Such fields include optics, hard disc manufacture, micro molding

and micro machining. Multi-axis machining and micro-fabrication techniques are seeing surfaces with sub-micron form accuracy and the production of nano-scale surface features. With ever decreasing manufacturing scales the current state of online metrology methods is found to be lacking. Light scattering methods are numerous and well established, they can give a qualitative idea of overall surface roughness and are in generally suitable for in-situ measurement. Unfortunately they cannot provide traceability as they work using fitting and statistical interpretation. Additionally, they are all area averaging techniques and so cannot be used to discern micro-structures [1-4].

A variation of phase shifting interferometry has been developed using a combination of a swept wavelength laser light source coupled with Fourier analysis of the returned signal periods to provide a real time 3D profile of a surface; its major drawback however is its lack of height resolution (approx 1μm) and as such is unsuitable for nano-scale manufacturing requirements [5]. Another method that has been developed recently uses analysis of the Fraunhofer diffraction pattern formed from a surface. Accurate results have been obtained using this method but it is currently only possible to measure isotropic surfaces with known periodic structures [6].

Optical interferometric techniques for metrology hold many advantages such as speed, resolution, traceability and non-contact measurement. They are not however very suitable for the application to on-line measurement due to the fact that any height disturbance is mapped directly onto the measurement result. This research hopes to try and alleviate this issue by providing immunity to disturbance during the measurement interval by way of active vibration compensation, thus realizing an instrument with the benefits of an optical interferometer, but which is suitable for on-line applications.

One of the central requirements for the development of the multiplexed fiber interferometer is the ability to place it on-line, in a workshop environment. Clearly such a requirement presents difficulties for precision measurement where usually the environment is a vibration isolated, temperature stabilized clean room. The challenge to try and create a device to measure accurately and repeatedly under workshop conditions is a major one.

2. Principle

The key feature of the multiplexed fiber interferometer is the combination of two interferometers operating at different wavelengths but which follow a common path for the majority of their length. The paths separate only at the optical probe, at which point they are laterally displaced along a profile on the measurand surface. Any vertical movement of the measurand due to vibration will change the optical path length of both interferometers equally. Additionally, any path length change elsewhere in the interferometer due to temperature variation will also affect both interferometers equally.

Using one of the interferometers as a reference interferometer at a fixed wavelength, we can measure the fluctuations in optical path length due to these external factors. Furthermore, the use of an actuator to alter the path length in one of the arms will induce an identical path length change in both interferometers. Closed loop control can be applied using the fixed wavelength reference interferometer output as the feedback source. When employed, the closed loop control can lock the reference interferometers path length at any point and hold it there in the face of disturbance. By virtue of the near common path configuration, this will in effect hold the second, measurement interferometer steady as well. This measurement interferometer is now free to perform the required measurement in a stable fashion [7].

The reference interferometer also provides the ability to implement accurate phase shifting interferometry techniques in order to retrieve the phase data from the measurement interferometer output. The mirror may be moved very accurately using the same closed loop feedback method as for vibration cancellation.

The actual surface measurement is performed by sweeping the light beam of the measurement interferometer along a profile on the surface. This is facilitated by tuning the source wavelength, and placing a blazed diffraction grating in the beam path. The first order beam is thus used as an optical stylus. The interference signal is sampled and digitized during the sweep to provide a discrete set of intensity values for each sampled point on the swept profile.

3. Apparatus

Figure 1 shows the experimental setup of the interferometer. A laser diode and the tunable laser (Ando Electric Co. AD4320D) illuminate the reference and measurement interferometers respectively. The laser diode operates at a wavelength of 1550nm and the TLS is operated between 1560 nm and 1580 nm. Both sources are multiplexed into the same fiber by a 3dB coupler. A combination of a reflective diffraction grating and collimating objective lens provides the ability to scan the measurement beam across the surface of the measurand, by tuning the source wavelength. De-multiplexing of the two interferometer sources is performed by a combination of a circulator and fiber bragg grating (FBG). After de-multiplexing, the intensity of each interference signal is interrogated by a fiber pigtailed PIN detector.

The actual interferometer is a Michelson configuration using a blazed diffraction grating (Jobin Yvon 510 97 020) with the reflected zero order beam and the diffracted first order beam providing the two beam paths. Light from the input fiber is collimated onto the diffraction grating using a graded index (GRIN) lens, which serves also to couple the returning light beam

back into the fiber. On retro-reflection from the reference mirror and the measurand surface, they recombine on the grating. A blazed grating is used to shift more of the source light power to the measurand (first order) surface beams as it is reasonable to expect that this surface would generally be less reflective than the reference mirror. An achromatic doublet (Melles Griot LAI007) is used to collimate the diffracted beam onto the measurand surface. When the wavelength of the diffracted beam is tuned the measurement beam sweeps laterally across the surface. Clearly, the lateral resolution of the instrument is a limited by the focused measurement beam diameter. The wavelength change, $\Delta\lambda$ of the tunable laser (Ando Electric Co. AD4320D) is from 1560 nm to 1580 nm. This yields an approximate scan path length, S of;

$$S = f \cdot \frac{\Delta\lambda}{d\cos\beta} \tag{1}$$

Where β is the first order diffraction angle, d the grating pitch, $\Delta\lambda$ the wavelength change and f the effective focal length of the lens. The angle of diffraction of the first order was set to approximately 70º by altering the angle of incidence of the beam, thus we will use a constant of $\beta = 70°$. For a grating pitch, $d = 1/900\times10^{3} m$ at a focal length of $f = 56.7mm$ we have a total scan length of approximately 3mm.

A data acquisition (DAQ) card (National Instruments NI PCI-6221) samples the measurement interferometer output during the wavelength sweep generating a data array with each element representing the interferometer intensity at each point on the scanned profile. The reference interferometer measurement beam remains in the same spot on the surface during the profile scan since its wavelength remains constant at 1550 nm. It is this reference interferometer output, de-multiplexed by the FBG, which provides the feedback for the closed loop control, enabling both active vibration compensation and phase shifting to take place simultaneously.

A combination of a fiber optic circulator and an FBG is used in order to de-multiplex the outputs of the two interferometers. The attenuation outside of the 1550nm pass band on reflection by the FBG is around 25dB. This effectively separates the reference interferometer source wavelength from the tuned wavelength range sourcing the measurement interferometer. They are analyzed separately by the electronics using two separate PIN detectors. The PIN detectors are operated with no reverse voltage bias in order to reduce excess shot noise resulting from any dark current flow. This is reasonable as high speed operation is not a priority in this application. Each PIN detector is interrogated by transimpedance amplifier which provides high gain current to voltage conversion.

State of polarization (SOP) evolution in single mode optical fibers can be a major source of error in any interferometric optical fiber sensor. The subject has been well studied and many methods for overcoming such effects have been suggested [8]. The arms of a fiber interferometer can be modeled as a lumped birefringence R_{r-m} of rotational magnitude (phase delay) Ω_{r-m}. The visibility of the interferometer output is a function of the angle, θ subtended by the great circle joining the input SOP and the lumped birefringence $R_{r-m}(\Omega_{r-m})$, as represented on the Poincaré sphere [9]. In the case for our instrument, the arms are free space optics thus $R_{r-m}(\Omega_{r-m})$ remains approximately static. As such it is only the variation of the input SOP that alters the value of θ. The dependence of visibility on θ is seen to be,

$$V = \left\{1 - \sin^2\theta \cdot \sin^2\left(\Omega_{r-s}/2\right)\right\}^{1/2} \tag{3}$$

It has also been shown that phase error in the output of an interferometer may also be produced by SOP variation and that this phase error is most pronounced when the visibility is at a

minimum. Thus the best operating conditions for a fiber interferometer in terms of both signal to noise ratio and polarization induced phase noise is to ensure that the visibility is maximized.

Pseudo un-polarized light as produced by a polarization scrambler, assuming the frequencies or interest are much lower than the scrambling frequency, can be used to reduce visibility variance due to SOP evolution in the input fiber. We used an all-fiber polarization scrambler () which has a scrambling rate of 200 kHz. This resulted in a much improved stability from input lead perturbation at the cost of slightly reduced visibility. In addition, all fibers were taped down to the optical table in order to reduce movement wherever possible. Currently, the position of a fiber loop on the optical table is adjusted to obtain an approximate maximum visibility value before the scrambler is switched on [10].

4. Phase Retrieval

Extraction of phase data from the output of an interferometer is non-trivial due the co-sinusoidal nature of the response. Phase shifting interferometry (PSI) is one solution to retrieving the absolute phase value from an interferogram. Algorithms for this technique have been well researched and a multitude have been developed e.g. Carré, Schwider-Hariharan, 3-step methods, 5-step methods etc. They each offer different advantages; the Schwider-Hariharan is relatively insensitive any phase shifting error while the Carré does not require a specific value phase shift for instance. In general, the more steps used the less sensitive the algorithm is to intensity noise in the data [11-13].

In our method the measurement interferometer source wavelength is tuned to provide the beam scanning, and the resulting intensity values produced by the scanned profile are sampled. After each beam sweep, a phase shift is induced by moving the piezo-electric translator (PZT) mounted reference mirror. We thus retrieve four sets of intensity data, each containing the

intensity values for the same scanned profile but at different phase shifts. The Carré algorithm was used in preference to other methods because it is unique in the fact that it does not require a known phase shift to be performed, only that the four phase shifts are identical. This is clearly a great advantage in this system as the displacement of the mirror will induce a different magnitude of phase shift in each of the tuned wavelengths used to gain the whole scan profile.

If $\varphi(x)$ is the original phase at a sampled point x on the scan profile, the phase is altered by 4 equal steps; -3α, -α, α and 3α around this point and 4 intensity values are obtained, $I_1(x), I_2(x), I_3(x)$ and $I_4(x)$ respectively. These can then be input into the Carré algorithm to yield the original phase value at each point, x;

$$\varphi(x) = \tan^{-1}\sqrt{\frac{\left(3I_2(x)-3I_3(x)-I_1(x)+I_4(x)\right)\left(I_1(x)+I_2(x)-I_3(x)-I_4(x)\right)}{\left(I_1(x)-I_2(x)-I_3(x)+I_4(x)\right)^2}} \tag{4}$$

The most effective phase shifting angle to provide the greatest immunity from random, non-systematic intensity noise (thus reducing lost data points) has been shown to be 110° thus α is set to 55° [14].

The active vibration compensation is performed by a combination of an analogue opamp based proportional-integral controller coupled with a PZT, on which the reference mirror is mounted. Both interferometers use the same reference mirror so the act of stabilizing the reference interferometer simultaneously stabilizes the measurement interferometer by virtue of their common paths.

With closed loop control it is possible to lock the reference interferometer at any point on the reference fringe simply by adjusting the set-point voltage applied to the proportional-integral controller. This holds an obvious advantage for the purpose of accurately moving the reference

mirror during phase shifting. Non-linearities present in all PZTs such as hysteresis and creep are now greatly reduced and accuracy is greatly enhanced. A low voltage PZT stack is utilized (PI 820.10) which provides a displacement of 15μm/100V. This means with a ±15V control voltage range we can apply approximately 4.5μm of displacement thus providing 6 full fringes of compensation range.

In order to calculate the required set point voltages for the phase stepping, a ramped voltage signal is applied to the PZT in order to move the reference interferometer output over several fringes. The peaks, V_{pk-lo} and V_{pk-hi} of the resulting sinusoidal output from the interferometer are then detected. The setpoint voltage, V_{out} relating to any required phase shift value, φ may then be calculated using the following formula;

$$V_{out} = V_{pk-lo} + \frac{V_{pk-hi} - V_{pk-lo}}{2}(1+\cos\varphi) \tag{5}$$

The required setpoint values are calculated in software and then output to the proportional-integral controller when necessary using an analog output present on the DAQ card. This routine is run prior to each measurement cycle.

5. Results

In order to determine the effectiveness of the vibration compensation two experiments were carried out. First, a sinusoidal disturbance of 300nm peak to peak was applied to the measurement mirror using a PZT. The disturbance was centered about the quadrature point and its magnitude recorded. The active vibration compensation was then switched on and the interferometer was then locked to the quadrature point, a reduced magnitude being observed. The experiment was repeated at gradually increasing frequencies. Figure 2 shows the attenuation of

the disturbance observed at the output of the measurement interferometer when the vibration compensation was switched on relative to the uncompensated signal. The reduced effectiveness of the vibration compensation at the higher frequencies is due to the limited slew rate of the PZT. This could be improved by using a stiffer pre-loaded PZT and applying the full scale voltage range with a suitable PZT driver.

Figures 3(a) and (b) show the fast Fourier transform (FFT) output from a digitizing oscilloscope of the measurement interferometer signal with an applied sinusoidal disturbance of 200Hz and 300nm peak to peak, compensation is switched off and on respectively. The DC present is due to the bias intensity present at the interferometer output. Figure 4 shows the action of the active vibration stabilization on an induced full-fringe disturbance at 10Hz. The left half of the graph shows the effect of the disturbance on the reference interferometer output disturbance. At the midpoint the controller is switched on and set to the quadrature point, the right half of the graph shows the now stabilized output. The data was recorded at a sample rate of 2 kHz.

A second experiment was carried out to determine the ability of the system to take measurements in the face of induced disturbance. A step height sample measured with the system. A large scale 50Hz sinusoidal disturbance of 750nm peak to peak was applied to the measurand. Such a disturbance accounts for approximately a full fringe of disturbance around the operating wavelength and as such would completely obscure any height data obtained in any uncompensated interferometer. The step height was first measured by the interferometer with no disturbance applied and the resultant phase profile is shown in figure 5a. It was then measured again with the disturbance applied to the measurand; the results are shown in figure 5b. Due to the fact that the phase stepping and the active vibration compensation are both controlled by the same closed loop feedback, it is impossible to make a measurement without also having the

vibration compensation active. We cannot therefore show the worst case result of the disturbed step height sample with no vibration compensation present.

6. Discussion

A novel optical interferometric instrument for the measurement of nano-scale surfaces in the face of severe environmental disturbance has been demonstrated. Measurement is provided by beam scanning using a blazed diffraction grating and a tunable laser source. A single wavelength laser diode provides a second interferometer, with a near common path configuration with the measurement interferometer, providing active vibration compensation and accurate phase shifting. The Carré PSI algorithm is used to derive the actual phase from four phase shifted intensity profiles. Disturbance reductions of approximately 13dB were observed at low frequencies with the response dropping off rapidly after 200Hz.

Finally, a step height sample was measured in the face of an applied full fringe disturbance that would have completely obliterated results from an uncompensated interferometer. More effective compensation could be provided the use of a stiffer, pre-loaded PZT and higher driving voltage range.

The next stage of our work is to replace the PZT and mirror with an electro-optic phase modulator. This will allow the path length to be changed without any mechanical movement. The very high frequency response of electro-optic devices will allow much higher loop gains and should extend the effective vibration compensation range greatly.

References

1. T. Vorburger, and E. Teague, “Optical techniques for on-line measurement of surface topography,” Precis. Eng. 3(2), 61-83 (1981).
2. T.Vorburger, E. Marx, and T. Lettieri, “Regimes of surface roughness measurable with light scattering,” Appl. Opt. 32, 3408 (1993).
3. K. Creath, “Phase-shifting speckle interferometry,” Appl. Opt. 24, 3053-3058 (1985).
4. C. Tay, S. Wang, C. Quan, and H.Shang , “In situ surface roughness measurement using a laser scattering method,” Opt. Commun., 218, 1-10 (2003).
5. S. Kuwamura, and I. Yamaguchi, “Wavelength scanning profilometry for real-time surface shape measurement,” Appl. Opt. 36, 4473-4482 (1997).
6. A. Taguchi, T. Miyoshi, Y. Takaya, and S. Takahashi, “Optical 3D profilometer for in-process measurement of microsurface based on phase retrieval technique,” Precis. Eng. 28, 152-163 (2004).
7. X. Jiang, K. Wang, and H. Martin, "Near common-path optical fiber interferometer for potentially fast on-line microscale-nanoscale surface measurement," Opt. Lett. **31**, 3603-3605 (2006).
8. A. Simon, and R. Ulrich, “Evolution of polarisation along a single-mode fibre,” App. Phys. Lett. 31, 517-520 (1977).
9. M. Johnson, “Poincaré representation of birefringent networks,” Appl. Opt. 20, 2075-2080 (1981).
10. A. Kersey, M. Marrone, and A. Dandridge, “Analysis of Input-Polarization-Induced Phase Noise in Interferometric Fiber-optic Sensors and Its Reduction using Polarization Scrambling,” J. Lightwave Technol. 8, 838-845 (1990).

11. K. Creath, "Phase-Measurement Interferometry Techniques," in *Progress in Optics*. XXVI, E. Wolf, ed. (Elsevier Science Publishers, Amsterdam, 1988), pp. 349-393.
12. P.S. Huang, and S. Zhang, ”Fast three-step phase-shifting algorithm”, Appl. Opt. 45, 5086-5091 (2006).
13. J. Schwider, R. Burow, K. Elssner, , J. Grzanna, R. Spolaczyk, and K. Merkel, “Digital wave-front measuring interferometry: some systematic error sources,” Appl. Opt. 22, 3421-3432 (1983).
14. K.M. Qian, F.J. Shu, and X.P. Wu, “Determination of the best phase step of the Carré algorithm in phase shifting interferometry,” Meas. Sci. Technol. 11, 1220–1223 (2000).

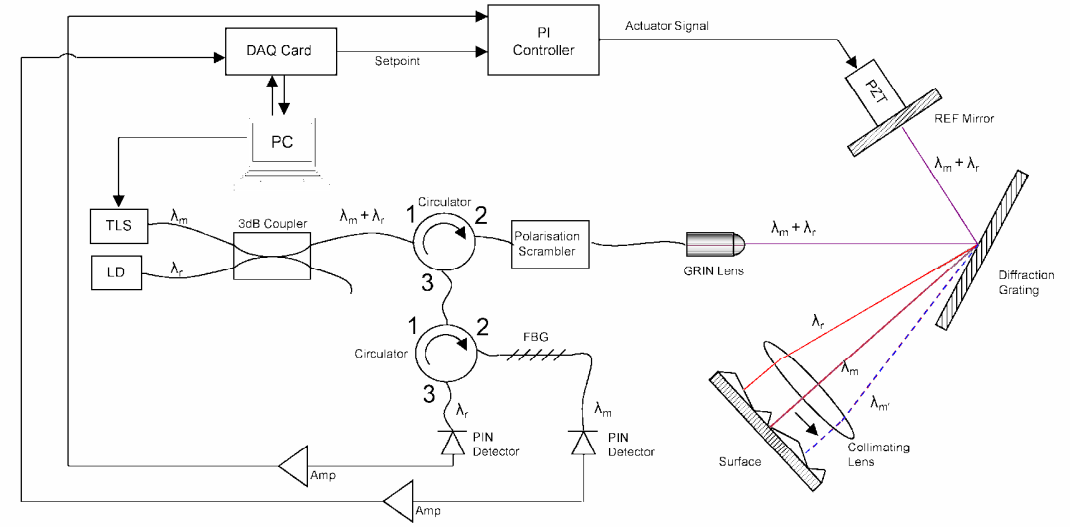

Fig. 1. Experimental Setup

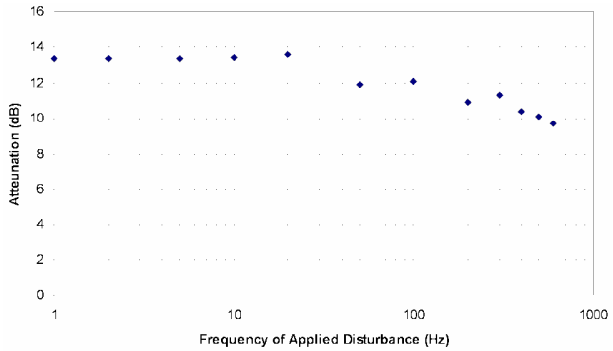

Fig. 2. Attenuation of a 300nm peak to peak induced disturbance

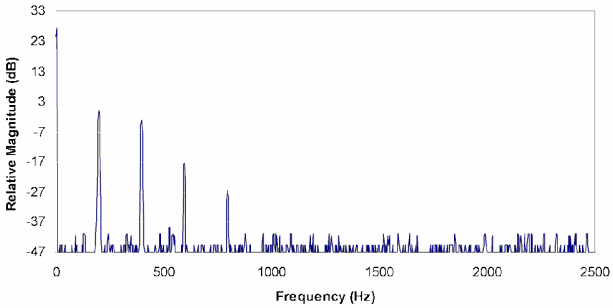

Fig. 3(a). Frequency response of uncompensated interferometer

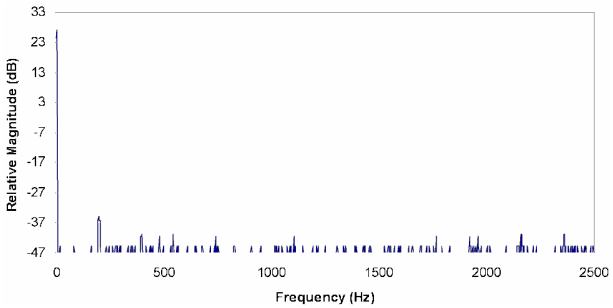

Fig. 3(b). Frequency response of compensated interferometer

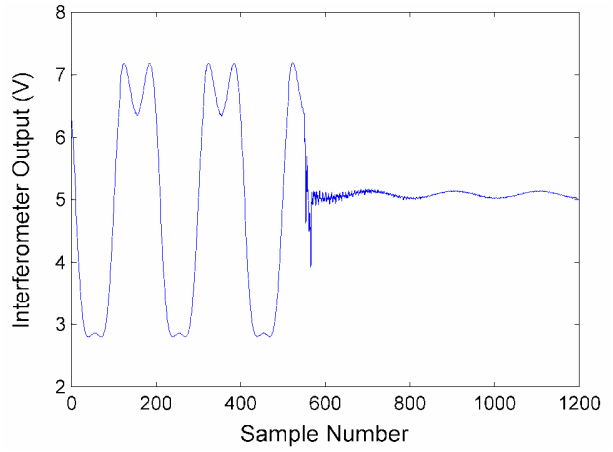

Fig. 4. Effect of active vibration compensation on a 10Hz full scale sinusoidal disturbance

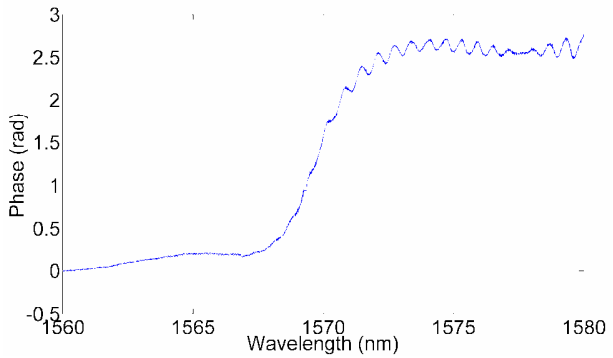

Fig. 5(a). Scanned step height with no disturbance

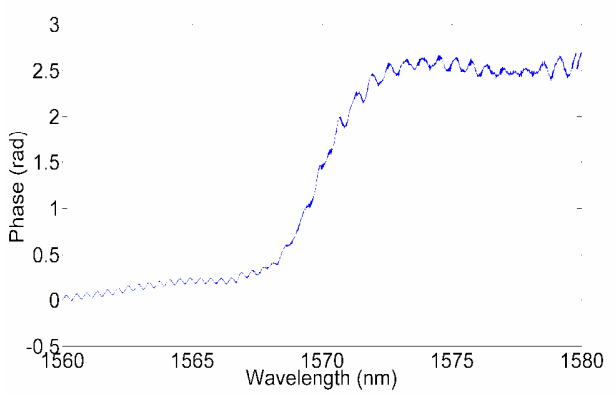

Fig. 5(b). Scanned step height with 750nm peak to peak induced disturbance

Fig. 2. Experimental Setup

Fig. 2. Attenuation of a 300nm peak to peak induced disturbance

Fig. 3(a). Frequency response of uncompensated interferometer

Fig. 3(b). Frequency response of compensated interferometer

Fig. 4. Effect of active vibration compensation on a 10Hz full scale sinusoidal disturbance

Fig. 5(a). Scanned step height with no disturbance

Fig. 5(b). Scanned step height with 750nm peak to peak induced disturbance